JOURNAL OF GEOPHYSICAL RESEARCH: SPACE PHYSICS, VOL. 118, 542–553, doi:10.1029/2012JA018235, 2013

East-west differences in *F*-region electron density at midlatitude: Evidence from the Far East region

Biqiang Zhao,[1,2,3] Min Wang,[4] Yungang Wang,[5] Zhipeng Ren,[1,2] Xinan Yue,[5] Jie Zhu,[1,2,7] Weixing Wan,[1,2] Baiqi Ning,[1,2] Jing Liu,[1,2,7] and Bo Xiong[1,2]

Received 25 August 2012; revised 15 October 2012; accepted 19 November 2012; published 31 January 2013.

[1] The global configuration of the geomagnetic field shows that the maximum east-west difference in geomagnetic declination of northern middle latitude lies in the US region (~32°), which produces the significant ionospheric east-west coast difference in terms of total electron content first revealed by Zhang et al. (2011). For verification, it is valuable to investigate this feature over the Far East area, which also shows significant geomagnetic declination east-west gradient but smaller (~15°) than that of the US. The current study provides evidence of the longitudinal change supporting the thermospheric zonal wind mechanism by examining the climatology of peak electron density (NmF2), electron density (Ne) of different altitudes in the Far East regions with a longitude separation of up to 40–60° based on ground ionosonde and space-based measurements. Although the east-west difference (R_{ew}) over the Far East area displays a clear diurnal variation similar to the US feature, that is negative R_{ew} (West Ne > East Ne) in the noon and positive at evening-night, the observational results reveal more differences including: (1) The noontime negative R_{ew} is most pronounced in April–June while in the US during February–March. Thus, for the late spring and summer period negative R_{ew} over the Far East region is more significant than that of the US. (2) The positive R_{ew} at night is much less evident than in the US, especially without winter enhancement. (3) The magnitude of negative R_{ew} tends to enhance toward solar maximum while in the US showing anticorrelation with the solar activity. The altitude distribution of pronounced negative difference (300–400 km) moves upward as the solar flux increases and hence produces the different solar activity dependence at different altitude. The result in the paper is not simply a comparison corresponding to the US results but raises some new features that are worth further studying and improve our current understanding of ionospheric longitude difference at midlatitude.

Citation: Zhao, B., M. Wang, Y. Wang, Z. Ren, X. Yue, J. Zhu, W. Wan, B. Ning, J. Liu, and B. Xiong (2013), East-west differences in *F*-region electron density at midlatitude: Evidence from the Far East region, *J. Geophys. Res. Space Physics*, *118*, 542–553, doi:10.1029/2012JA018235.

1. Introduction

[2] In recent years, there has been a growing interest regarding the longitudinal dependence of the ionosphere and thermosphere. At low and equatorial latitudes, numerous studies have shown that the ionospheric and thermospheric parameters, such as the plasma density, equatorial electrojet (EEJ), the vertical E × B plasma drifts, the electron temperature, the nitric oxide density in the low thermosphere, and *F*-region zonal neutral wind, show obvious longitudinal structures [cf. *England*, 2011, and references therein]. The physical mechanism responsible for the observed phenomenon is mainly due to the upward propagating of the diurnal nonmigrating tide, modifying the dynamo electric field to produce longitudinal variability in the equatorial fountain effect [e.g., *Immel et al.*, 2006; *Hagan et al.*, 2007]. Although the source of this longitude difference is not directly associated with the geomagnetic field configuration, the intermediate dynamo process is indeed coherent to the horizontal magnetic field at the magnetic equator. At midlatitudes, another kind of

[1]Key Laboratory of Ionospheric Environment, Institute of Geology and Geophysics, Chinese Academy of Sciences, Beijing, China.
[2]Beijing National Observatory of Space Environment, Institute of Geology and Geophysics, Chinese Academy of Sciences, Beijing, China.
Corresponding author: B. Zhao, Key Laboratory of Ionospheric Environment, Institute of Geology and Geophysics, Chinese Academy of Sciences, Beijing 100029, China. (zbqjz@mail.iggcas.ac.cn)

2169-9380/13/2012JA018235

[3]State Key Laboratory of Space Weather, Chinese Academy of Sciences, Beijing, China.
[4]Institute of Earthquake Science, China Earthquake Administration, Beijing, China.
[5]National Center for Space Weather, China Meteorological Administration, Beijing, China.
[6]COSMIC Program Office, University Corporation for Atmospheric Research, Boulder, Colorado, USA.
[7]University of Chinese Academy of Sciences.

longitude variability in the ionosphere named the Weddell Sea anomaly (WSA), characterized by an evening enhancement in electron density in summer (actually including equinox months) usually exceeding the noon value, was raised by *Horvath and Essex* [2003]. It was later renamed by *Thampi et al.* [2009] and *Lin et al.* [2009, 2010] as the midlatitude summer nighttime anomaly (MSNA) because of its northern counterparts near the northeast Asia and Europe/Africa regions, *Liu et al.* [2010] called it the phase reversal of diurnal anomaly, and *Burns et al.* [2011] named it summer evening anomalies (SEAs) in a more general concept, which is proved to be directly related to the geomagnetic field configuration.

[3] The physical mechanism for WSA (or MSNA) formation in the earlier research was assumed to be the combined effect of the longer summer sunlight hours and the day-to-night/summer-to-winter equatorward neutral winds as WSA takes place in the longitude sectors where the dip equator excurses farthest toward the geographic pole [*Kohl and King*, 1967; *Rishbeth and Garriott*, 1969; *Dudeney and Piggott*, 1978; *Horvath and Essex*, 2003]. Later, a number of researches emphasized that the contribution of the zonal wind with the declination to the vertical component of the effective neutral wind cannot be neglected at dusk, which is capable of transporting the plasma along the magnetic field line [*Luan and Solomon*, 2008; *Jee et al.*, 2009; *He et al.*, 2009, 2011; *Ren et al.*, 2012]. *Jee et al.* [2009] found that the seasonal variations of the WSA are physically consistent with the seasonal characteristics of the neutral winds further supporting the wind lifting mechanism. However, *Burns et al.* [2008] pointed out that if the zonal wind prevails around dusk as suggested by *Dickinson et al.* [1981], the wind process would not be significant at driving the WSA. In addition to this neutral wind process another mechanism can also affect the WSA. For example, *Evans* [1965] suggested that the rapid fall of electron temperature at sunset causes the downward motion of the ionization from above the F2 peak and from the plasmasphere, and leads to an increasing of plasma near and above the F2 peak. To study which mechanism is more important, *Chen et al.* [2011, 2012] on the basis of the SAMI2 model, found that equatorward neutral wind is identified as the major cause of the WSA, while the downward flux from the plasmasphere provides an additional plasma source to enhance or maintain the density of the anomalous structure.

[4] More recently, *Zhang et al.* [2011] reported a new finding of pronounced longitudinal variations in midlatitude total electron content (TEC) over the continental US manifested as an east-west coast difference, based on observations of ground-based GPS receivers. The phase of the east-west difference depends on the local time. The proposed physical mechanism of this phenomenon, an analogy of WSA or MSNA, is the varied magnetic declination over the US along with the behavior of thermospheric zonal winds and, in particular, their diurnal variations. The meaning of this study lies in that longitudinal variations for some regions in ionospheric electron density contain critical information on thermospheric zonal winds, which can be used to derive zonal winds. *Zhang et al.* [2012b] has shown a good linear relationship between the east-west differential ratio in plasma density Ne at 400 km and the Fabry-Perot interferometer eastward winds over Millstone Hill during the nighttime. Such idea resembles the work of *Karpachev and Gasilov* [2001, 2006], which have derived zonal and meridional wind components from Intercosmos-19 hmF2 measurements using the main principles ionospheric model developed by *Rishbeth et al.* [1978] called a servo model. In addition, as pointed out by *Zhang et al.* [2012a], this new longitude variability actually differs from the recent MSNA feature in that: (1) The MSNA is primarily an evening enhancement in plasma density relative to its daytime level, while the longitudinal change here shows a diurnal course. (2) The MSNA occurs most evident in summer time; the longitudinal difference occurs persistently in all seasons, without particular preference in summer.

[5] The global configuration of the geomagnetic field shows that the maximum east-west difference in geomagnetic declination over middle latitude lies in two longitude intervals, US 140°W–60°W and East Asia 60°E–140°E zones. The east-west asymmetry in geomagnetic declination for the US longitudes (~32°) is obviously larger than that of the East Asia longitudes (~15°) for typical midlatitude with inclination about 60–65°. Thus, it is valuable to investigate the east-west difference in the ionospheric parameters of the East Asia zone and compare the result with that of US region. If the mechanism of magnetic declination combined with the effect of thermospheric zonal winds is the primary drivers, the east-west asymmetry should be smaller than that in the US region. In this paper, we have investigated the diurnal, seasonal, solar cycle, and height dependency of the longitudinal variation of the ionosphere in the East Asia longitudes, more comprehensively than the previous work of *Wu et al.* [1998]. The paper demonstrates the similarity and discrepancy between the diurnal east-west asymmetry in the Eastern and Western Hemispheres and discusses the possible physical mechanisms.

2. Observation

[6] For the current study, we focus on observations made over the East Asia continent including three pairs of ionosondes distributed in the east and west of China, the electron density profiles (EDPs) derived from radio occultation (RO) technique of COSMIC/FORMOSAT-3 (a Constellation Observing System for Meteorology, Ionosphere, and Climate mission, here COSMIC for short), in situ plasma density measured from the Instrument Sonde de Langmuir (ISL) onboard the DEMETER satellite. A detailed description of the ISL measuring techniques relevant to its in situ satellite application on board DEMETER is given in *Lebreton et al.* [2006].

[7] The ionospheric F2 region critical frequency, foF2, is routinely scaled at the ionosonde stations in East Asia. The detailed information of each ionosonde station is given in Table 1 and the locations of the stations are illustrated in Figure 1. The geomagnetic declination and inclination are calculated from the 11th generation of International Geomagnetic Reference Field (http://www.ngdc.noaa.gov/IAGA/vmod/igrfhw.html). Data of Wakkanai (WK) and Alma ata (AA) are collected from the SPIDR website (http://spider.ngdc.noaa.gov/). History data of Changchun (CC) and Wulumuqi (WM) are obtained from China Research Institute of Radio wave Propagation. Beijing (BJ) and Kashi (KS) observatory are newly built ionosonde stations affiliated to the Beijing National Observatory of Space Environment of

Table 1. Information of the Used Ionosonde Stations

Station (Abbr.)	Latitude(°)	Longitude(°)	Magnetic Inclination (°)	Magnetic Declination(°)	Data Coverage
Wakkanai (WK)	45.40	141.70	59.1–59.2	–7.8 – –8.0	1958–1988
Alma ata (AA)	43.25	76.92	61.7–61.8	3.8–3.7	1958–1988
Changchun (CC)	43.83	125.27	60.1–60.1	–7.4 – –7.5	1964–1975
Wulumuqi (WM)	43.70	87.60	62.3–62.2	2.2–2.1	1964–1975
Beijing (BJ)	40.00	116.30	58.2	–5.7	2011
Kashi (KS)	39.70	76.20	58.8	3.1	2011

Institute of Geology and Geophysics in the Chinese Academy of Sciences and the National Center for Space Weather in China Meteorological Administration, respectively. The three pairs of ionosondes are grouped according to the criterion of minimum difference in geomagnetic inclination.

[8] The COSMIC constellation provides approximately 24 h local time coverage and 1000–2500 vertical EDPs (100–800 km) globally per day. The inversion of EDPs from RO observations is based on several assumptions, with the local spherical symmetry assumption being the most significant error source. The horizontal structures in some cases may significantly affect the retrieved profiles. Some statistical validations have showed good agreements with measurements of globally distributed incoherent scatter radars (ISRs) and ionosondes, especially at midlatitude area because of its relatively low horizontal gradient in Ne [e.g., *Schreiner et al.*, 1999]. This indicates that the COSMIC RO observations provide an unprecedented three-dimensional Ne data source for ionospheric physics studies. The reader is referred to *Schreiner et al.* [2007] and *Yue et al.* [2011] for a detailed description on the COSMIC mission and EDPs inversion technique. This database has attracted the interests of the community in the aspects of the ionospheric climatology and large-scale structure [e.g., *Liu et al.*, 2009; *Zhao et al.*, 2011].

[9] The French microsatellite DEMETER was launched on 29 June 2004 and put into a circular and quasi-Sun-synchronous orbit with an inclination of 98°. Descending and ascending nodes are at around 10:30 and 22:30 local time (LT), respectively. Altitude of DEMETER was 710, 680, and 660 km from June 2004 to December 2005, to January 2006, and to December 2010, respectively. The orbital period is about 100 min, and all longitudes are covered within ±65° geomagnetic latitude.

3. Result

3.1. Diurnal Variations and Seasonal Dependence in R_{ew}(NmF2)

[10] Figure 2a illustrates the diurnal variations of the observed 31 year monthly mean NmF2 in equinoctial and solstitial months at WK and AA during the interval 1958–1988, spanning two and a half solar cycles. To remove the magnetic activity effect, only the periods of $Kp < 4$ were considered. The error bar reflects the day-to-day variability associated with solar cycle variation. The blue empty circle denotes the ΔNmF2 ($NmF2_{WK} - NmF2_{AA}$) while the red dot refers to the hourly east-to-west differential index R_{ew} 5×10^5. The index R_{ew} is constructed through the procedure of *Zhang et al.* [2011], equivalent to a % east-to-west difference, where $R_{ew}(NmF2) = (NmF2_{east} - NmF2_{west})/(0.5 \times (NmF2_{east} + NmF2_{west}))$ and NmF2 data are hourly median values. The corresponding 31 year monthly maximum, mean, and minimum F10.7 are labeled in each subplot. It can be seen from the Figure 2a that during daytime (08:00–18:00 LT) NmF2 being higher at AA than at WK is most evident in June, less in September, and least in March and December, with daytime minimum R_{ew}(NmF2) approaches –0.4, –0.28, –0.05, and –0.12. At nighttime, the east-to-west difference is shown to have no seasonal preference with relatively higher R_{ew}(NmF2) reaching 0.2–0.3 after midnight in March and June. Figure 2b presents the same diurnal variations as Figure 2a but for CC and WM during the interval 1964–1975 spanning the 20th solar cycle. Note that CC and WM are separated by 37.67° longitude, which is much smaller than that of WK and AA (64.78°). It is shown that the east-to-west difference in NmF2 between CC and WM resembles the situation of WK and AA in Figure 2a, but with smaller value. The daytime negative difference is most evident in September, less in June, and least in March and December, with minimum R_{ew}(NmF2) approaches –0.25, –0.18, –0.05, and –0.02 under F10.7 = 110 sfu. The nighttime difference appears most evident in March and June after midnight with $R_{ew}(NmF2) = 0.2–0.23$. It is least evident in December.

[11] A more subtle seasonal variation in east-west difference for WK-AA and CC-WM are given in Figure 3, which shows R_{ew}(NmF2) as a function of the day of year (DOY) and LT. The data were binned for 30 day sliding average throughout the entire year. For WK-AA, it can be seen that the daytime negative R_{ew}(NmF2) exists during DOY 110–270 with first minimum value 0.5 appearing around DOY 150 and the second at DOY 240. The nighttime positive R_{ew}(NmF2) was shown to exist generally during DOY 30–300 that has two peaks in March and June with magnitude

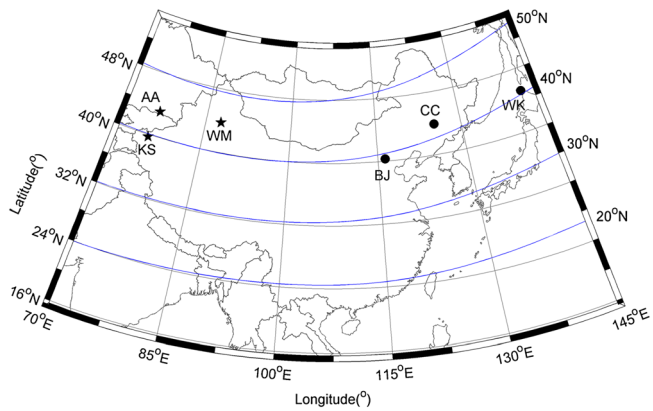

Figure 1. Locations of the stations listed in Table 1, and the blue lines represent the magnetic latitudes 20°N, 30°N, 40°N, and 50°N. The star and filled circle represent the west and east stations, respectively.

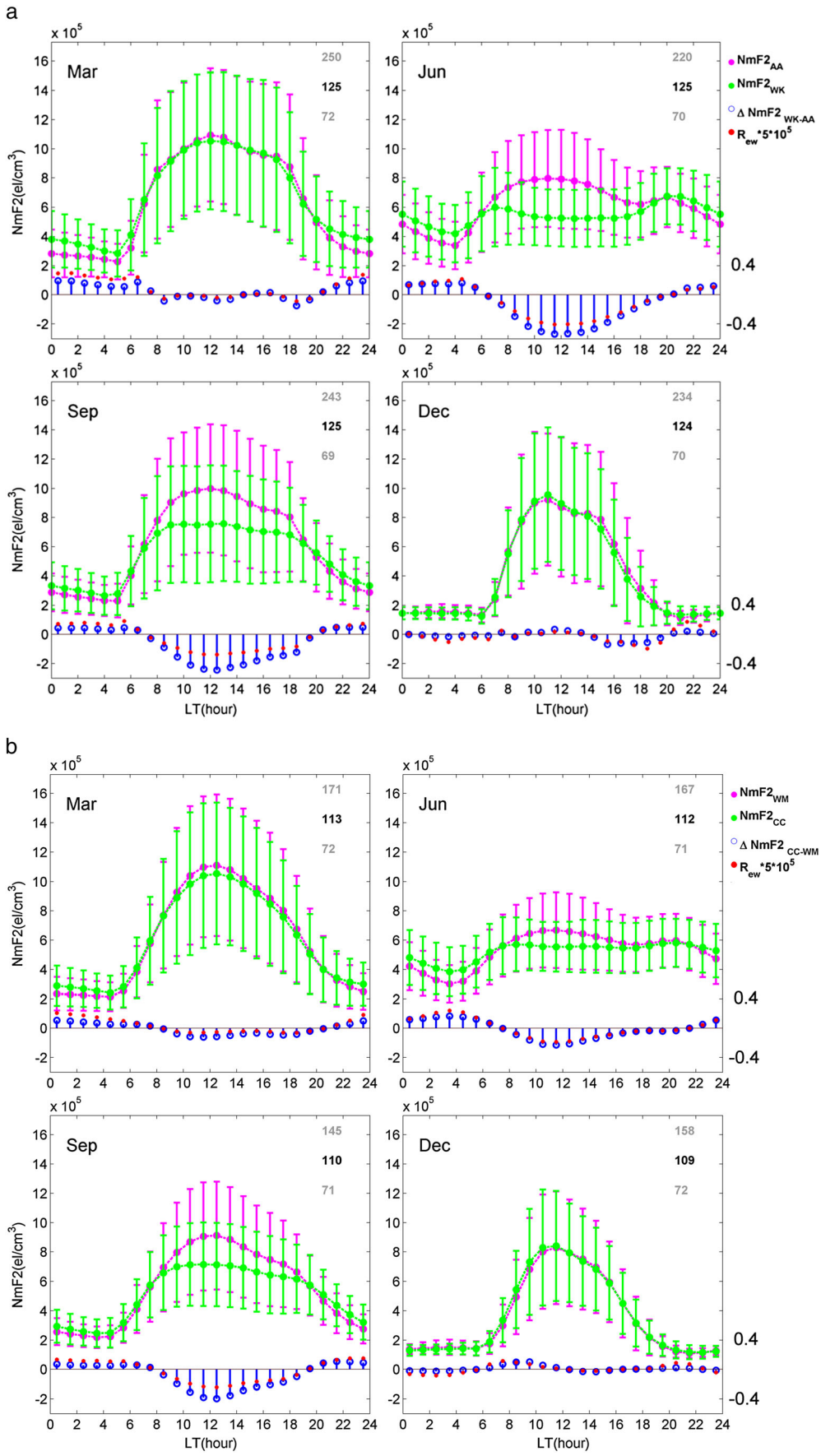
a
Mar
250
125
72
Jun
220
125
70
Sep
243
125
69
Dec
234
124
70
NmF2AA
NmF2WK
Δ NmF2 WK-AA
Rew*5*10^5
0.4
-0.4
NmF2(el/cm^3)
x 10^5
LT(hour)
b
Mar
171
113
72
Jun
167
112
71
Sep
145
110
71
Dec
158
109
72
NmF2WM
NmF2CC
Δ NmF2 CC-WM
Rew*5*10^5

Figure 2

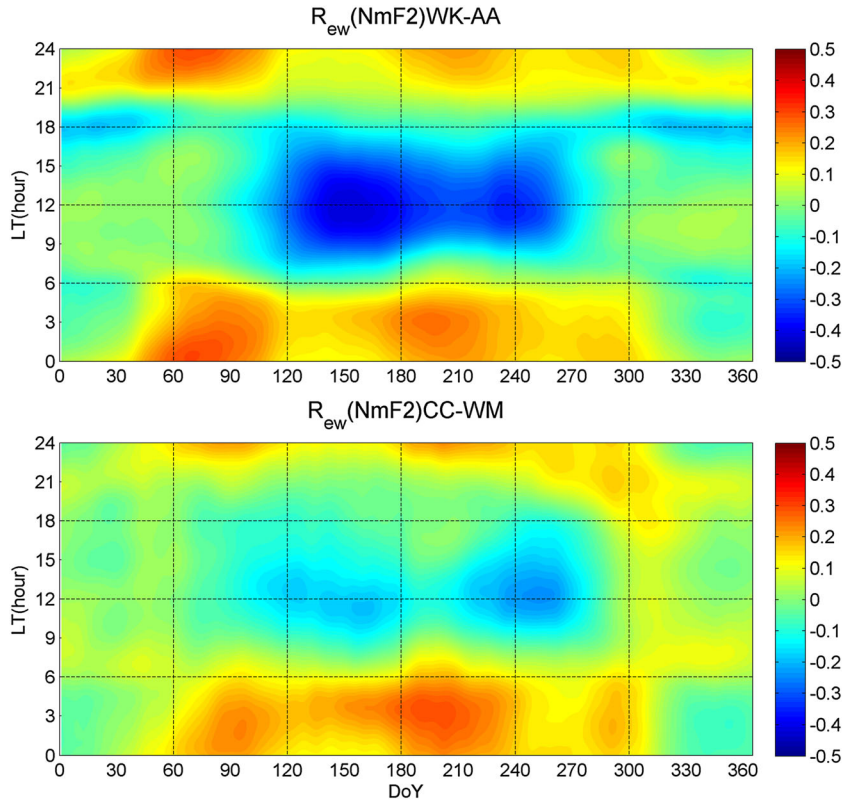

Figure 3. Averaged R_{ew}(NmF2) values as a function of DOY versus LT for WK-AA during 1958–1988 and CC-WM during 1964–1975.

around 0.2–0.3. For CC-WM, R_{ew}(NmF2) is much smaller but the distribution resembles that represented at WK-AA.

3.2. Solar Activity Dependence in R_{ew} (NmF2)

[12] Figure 4 shows the evolutions of east-to-west differential index R_{ew}(NmF2) for pair stations WK-AA and CC-WM as a function of local time and day number spanning solar cycles 19–22. The solar activity dependence of the overall patterns in the parameters of WK-AA is clearly seen in the figure. The diurnal minimum R_{ew}(NmF2) for WK-AA occurs in 1960 with value of –0.64. The diurnal maximum R_{ew}(NmF2) occurs in 1978 with values of 0.56. For CC-WM, the feature is not as clear as shown for WK-AA. The diurnal minimum R_{ew}(NmF2) for CC-WM occurs in 1968 with value of –0.46.

[13] To illustrate the solar activity dependence of east-to-west differential index more specifically, we have binned data into five groups of F10.7 level as the following: [0, 80], [80 120], [100 140], [120 160], [160 350]. Here we choose the minimum R_{ew}(NmF2) during 08:00–16:00 LT and maximum R_{ew}(NmF2) during 17:00–07:00 LT of WK-AA. For each F10.7 level, a seasonal variation is derived through 30 day moving average. The results, indicated in Figure 5, show clearly that the magnitude of the minimum R_{ew}(NmF2) increases with increasing solar activity and mainly occurs during DOY 150–240 and much less evident during rest days. One may also notice that as the solar activity increases, the lowest minimum R_{ew}(NmF2) occurs around DOY 130, with subminimum around DOY 255, and gradually shifts to one minimum around DOY 160. Furthermore, the difference between the low solar activity and high solar activity in R_{ew}(NmF2) reflects an enhanced semiannual component. In comparison, the relationship between the maximum R_{ew}(NmF2) and solar activity versus DOY is rather weak and complicated. The maximum R_{ew}(NmF2) value is shown to slightly increase with enhanced moderate solar activity during DOYs 0–90 and 240–330, and further reduced with increasing solar activity for the level F10.7 > 160. As a result, the solar activity does not seem to affect both maximum and minimum R_{ew} simultaneously, which accords with *Zhang et al.* [2012a] for the northern American region.

3.3. Altitude Dependence of East-West Asymmetry in Ne

[14] The altitude dependence of the east-to-west difference in Ne is investigated through the global observations of EDPs

Figure 2. (a) Local time (LT) variations of the observed 31 year monthly mean NmF2 at WK (green) and AA (magenta) in March, June, September, and December. The blue empty circle denotes the ΔNmF2 (WK-AA) while the red dot refers to the east-to-west differential index $R_{ew} \times 5 \times 10^5$. From top to bottom, the 31 year monthly maximum, mean, and minimum values of the 10.7 cm solar radio flux (F10.7 index) are labeled on the upper-right corner. (b) Same as Figure 2a but for CC (green) and WM (magenta) during the interval 1964–1975. The blue empty circle denotes the ΔNmF2 (CC-WM).

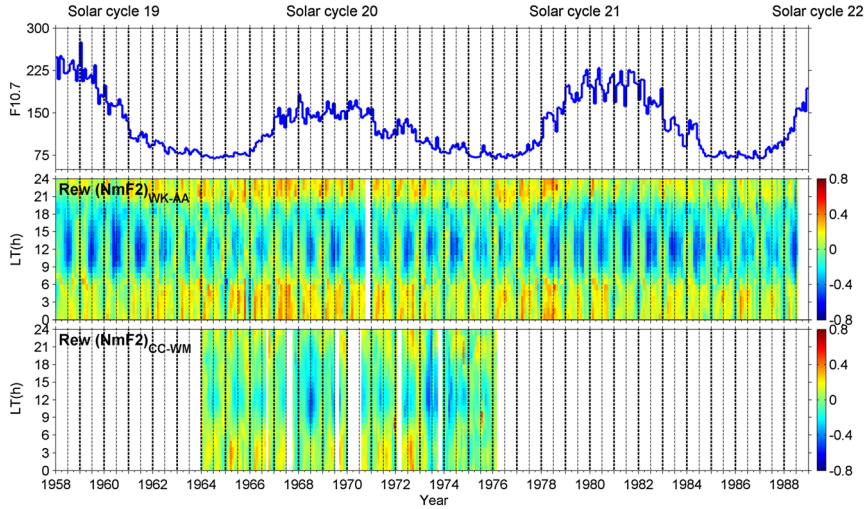

Figure 4. From top to bottom are the monthly mean values of F10.7 index, east-to-west differential index R_{ew}(NmF2)$_{WK\text{-}AA}$, and R_{ew}(NmF2) $_{CC\text{-}WM}$ during the period 1958–1988.

from the COSMIC satellites. We followed the procedure of *Lin et al.* [2010] to obtain the monthly averaged global ionospheric maps at various altitudes by taking median value of occultation soundings within each 5° by 5° grid in both longitude and latitude every 2 h during 40 days period (i.e., 5 days prior to and 5 days after each month). It is noted that only the data of $Kp < 4$ are taken to construct the ionospheric maps presented in this paper. We only present ionospheric maps in the 220–500 km altitude range, because some satellites were in the orbital lifting process and the microsatellites were at different altitudes during the early stage of the COSMIC project.

[15] In Figure 6 from top to bottom are columns of altitude-latitude profiles in Ne at longitude 135°E, 75°E, and east-to-west differential index R_{ew} for LT = 10:00, 12:00 ,. . ., 18:00, 20:00 during June 2007. It is clearly seen that the negative east-to-west difference in R_{ew} mainly occurs around 10:00–12:00 LT in the midlatitudes 30°N–65°N with the maximum value 0.8 centered at 50°N and ~350 km. The parameter hmF2 denoted by black shows that the west side *F* layer is 10–50 km higher than that of the east side where pronounced negative R_{ew} exists. The R_{ew} near the hmF2 is much lower than that of 100 km above, of which the value roughly reaches agreement with the NmF2 result. The positive R_{ew} actually reflects the intensity of the MSNA that accords well with the result of *Lin et al.* [2010]. Figure 7 presents the three-dimensional distribution of the plasma density over the Far East region at a fixed local time 12:00 LT with three slices representing the situation of Ne (Longitude = 60°E), Ne (Latitude = 50°N), and Ne (altitude = 250 km) respectively. The blue, red, and black dashed lines denote the negative, zero, and positive value of declination separately. The consecutive altitude-longitude and longitude-latitude variations in Ne show that there is an east-to-west gradient in Ne with a transition band existing around 90°E–100°E, which is clearly superimposed with the zero line in declination at midlatitudes. The distribution in Ne and configuration of declination are matched well. This result suggests a coherence between these two parameters which will be discussed in section 4.

[16] Figure 8 upper panels illustrate the altitude-latitude profiles of negative differential R_{ew} at 12:00 LT in summer month of different solar activity levels. For medium solar activity year 2012, we use the data of May–June instead because the daily number of RO events reduced from 2000–2500 in 2007 to ~1000 in 2012 due to the degraded performance of the COSMIC satellites. It is recognized that the region of pronounced negative east-west difference with $R_{ew} \leq -0.5$, 300–400 km, for the solar flux level F10.7 = 76 lifts entirely to 350–450 km for solar flux level F10.7 = 125. The centered minimum R_{ew} increases from 360 to 410 km. Thus, we can see that above 360 km, the

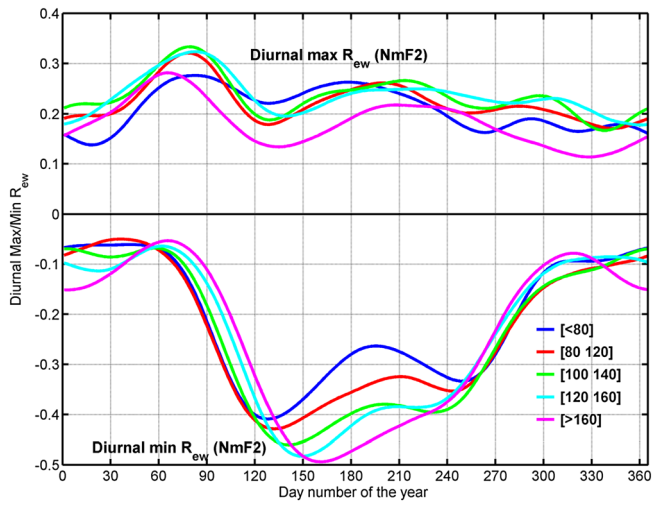

Figure 5. Seasonal and solar activity dependency of the diurnal maximum/minimum of east-west difference R_{ew} (WK-AA). The bottom curves are for the diurnal maximum R_{ew} ($NmF2_{East} > NmF2_{West}$), and the blue ones for the diurnal minimum R_{ew} ($NmF2_{East} < NmF2_{West}$). Results are given for five level groups of F10.7 solar flux units as a function of day number of the year.

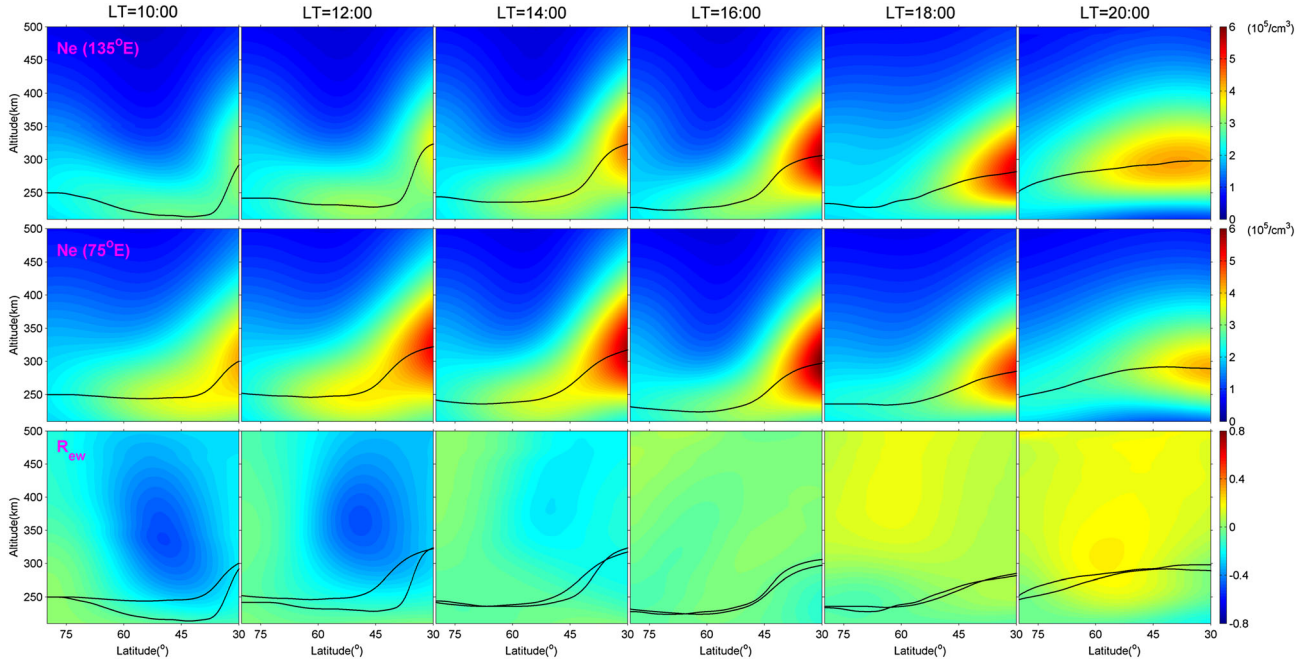

Figure 6. From top to bottom are the columns of Ne profiles at longitude 135°E, 75°E, and east-to-west differential index R_{ew} for LT = 10:00, 12:00, . . ., 18:00, 20:00 during the month June 2007. The parameter hmF2 denoted by black line is superimposed on each profile map.

R_{ew} for topside ionosphere shows a positive correlation with the solar activity while in the bottom side (250 km) remains constant or reduced slightly. This is opposite to the result of *Zhang et al.* [2012a] at a fixed altitude 400 km based on the ISR data, which shows a negative correlation. The R_{ew} of different altitudes should manifest different solar activity dependence. Because COSMIC is operated most of the time during low solar activity, further result is needed as the solar activity increases in the next 2 years reaching 24th solar cycle maximum. Figure 8 (bottom) shows the altitude-latitude profiles of positive differential R_{ew} at 20:00 LT. The maximum R_{ew}, 0.3, of low solar activity is centered at ~57°N and ~310 km and reduces a little and move upward slightly under moderate solar activity. Its altitude gradient is not as evident as that of negative R_{ew} at noon, and neither the solar activity dependence. This weak solar activity dependence is in agreement to the changes of positive R_{ew}(NmF2) in Figure 5.

[17] Furthermore, we also investigate the east-to-west asymmetry of the topside ionosphere at DEMETER altitude around 670 km. Monthly medians of Ne during 2007 June measured by DEMETER satellite are calculated for bins sized with 12° longitude and 8° latitude with shifting in the steps of 5° longitude and 3° latitude between ±60° geomagnetic latitude. Notice that the satellite altitude in the Northern Hemisphere varies between 665 and 675 km during the selected month. We constructed a map of R_{ew} (lon) as a function of longitude by setting R_{ew} (lon) = $(Ne_{lon}–Ne_{60°E})/(0.5 \times (Ne_{lon} + Ne_{60°E}))$. The spatial distributions of the R_{ew} (lon) for 10:00 and 22:00 LT are shown in Figure 9. The distribution of daytime negative R_{ew} in the topside ionosphere resembles that in the bottom side and *F* layer peak region with the minimum appearing at 130°E and 45°N–50°N; however, the magnitude –0.45 is smaller than that in the lower region (–0.8) as shown in Figure 6. The magnitude of positive R_{ew} (02–0.3) is comparable to that observed in the bottom side ionosphere from Ionosonde and RO measurements, which shows that the positive R_{ew} has no obvious altitude dependence.

4. Discussion

4.1. Comparison with the Results of US Region

[18] We have shown, from both the ground- and space-based instruments, that the ionosphere over the Far East region has large east-to-west differences at midlatitudes. The main features of this phenomenon and comparisons with the US region can be summarized as follows: (1) The most distinctive longitude difference in the Far East region is the large negative R_{ew} in the noon sector (West Ne > East Ne). The positive R_{ew} (East Ne > West Ne) at night is not evident and appear relatively higher in March and June, while in the US is much significant in winter and less evident in June. (2) The noontime negative R_{ew} in NmF2 is most pronounced in April–June while in the US for Ne at 350–450 km in the February–March period. Thus, for the late spring and summer period negative R_{ew} over the Far East region is more significant than that of the US especially during moderate and high solar activity. The second minimum appears around August–September for both regions. (3) The minimum negative R_{ew} in NmF2 tends to enhance toward increasing solar activity and the phase of minimum value shifts to the summer, while in the US negative R_{ew} shows anticorrelation with the solar activity. The positive R_{ew} has weak solar activity dependence. (4) The altitude distribution of pronounced negative R_{ew} mainly concentrates at 300–400 km and moves upward with the increased solar flux level, correspondingly leading to the different solar activity dependence of varied altitudes. Thus, the features of R_{ew} are quite different from

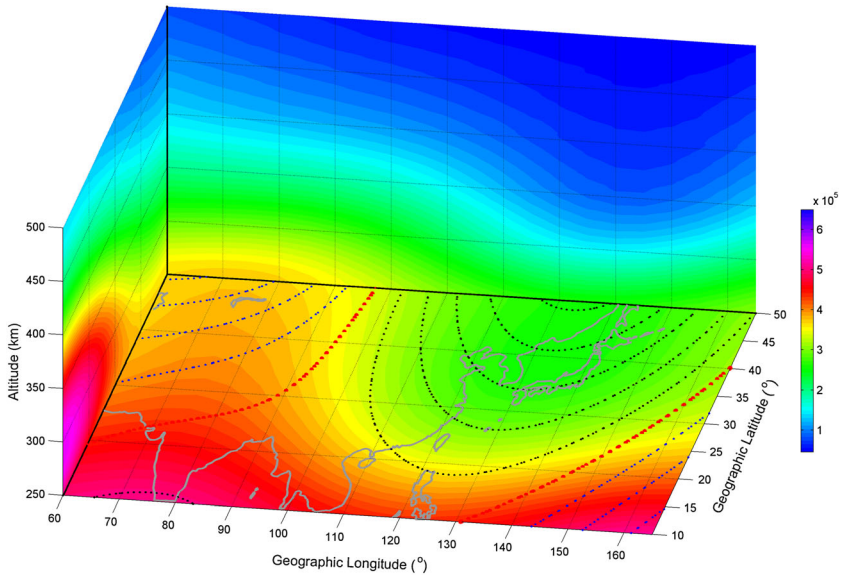

Figure 7. Three-dimensional distribution of the plasma density over the Far East region at a fixed local time 10:00 LT during June 2007 with three slices represent the situation of Ne (Longitude = 60°E), Ne (Latitude = 50°N), and Ne (altitude = 250 km), respectively. The blue, red, and black lines denote the positive, zero, and negative value of geomagnetic declination separately.

those shown in the US longitude [see *Zhang et al.*, 2012a, 2012b].

[19] Actually, the above comparisons with the results of the US region are not strict. To make an accurate comparison, the west and east observational sites should be of the same geomagnetic inclination, and the declination difference should also be equivalent. According to *Zhang et al.* [2012a, 2012b], the US east-west differences in electron density Ne at various *F* region heights were derived based on the Millstone Hill ISR observations with a longitude span from approximately –45°E to –95°E. Most data points were binned from (–51 ± 3°E, 47 ± 6°N) on the east side, and (–92°E ± 2°E, 48 ± 6°N) on the west side. The geomagnetic inclinations of the center points are 67° and 74° and declinations are –18.7° and 0.5° for the sample year 2008. The span of latitude bin seems too wide, which may introduce the error due to the ionospheric latitude variation especially if the data coverage is not uniform. In the Far East region we calculate the R_{ew} point-to-point while the geographic and geomagnetic latitude are nearly identical. The same

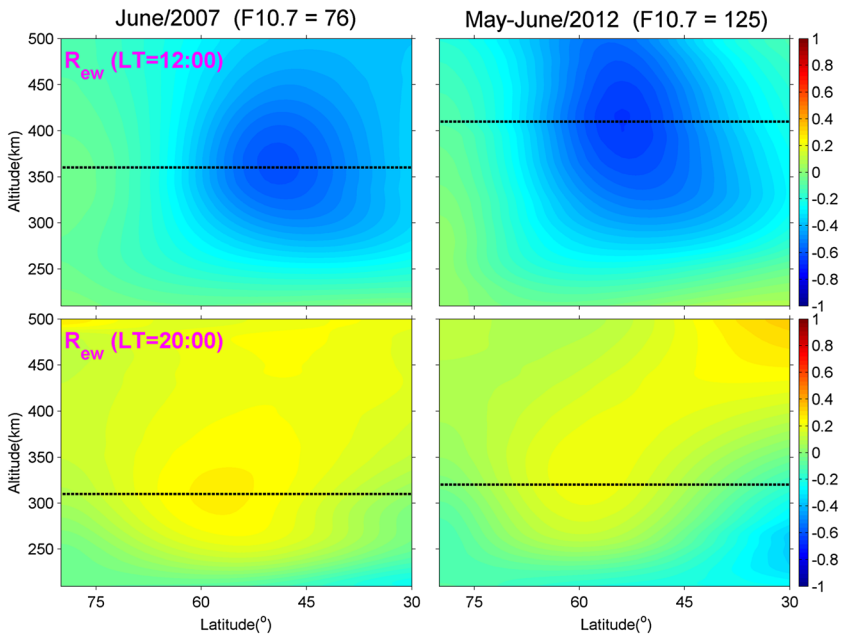

Figure 8. The altitude-latitude profiles of negative differential index R_{ew} at 12:00 LT and positive value at 20:00 LT during summer month with different solar activity levels in year 2007 and 2012.

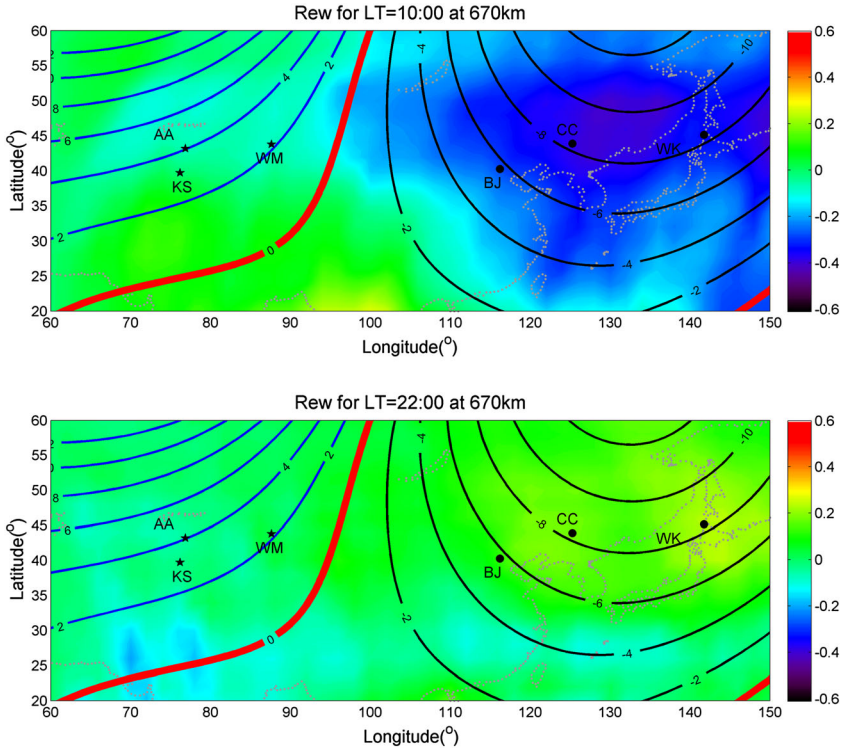

Figure 9. The longitude-latitude distribution of R_{ew} at 10:00 and 22:00 LT in June 2007 at topside ionosphere derived from DEMETER Ne measurement. The geomagnetic declination contour line and the stations in Figure 1 are superimposed on the map.

procedure should be adopted in the US longitude. Actually, we have selected several pairs of sites of the GPS TEC data with the situation the same as that used in the present study and an overall comparison has been made. The result, showing that the noontime negative R_{ew} in TEC is more significant in Far East Asian region than in the US during late spring and summer period at middle-high solar activity, agrees well with our present study. Detailed discussion and possible explanation will be made in our following work.

4.2. Possible Explanation for the Observed Feature

[20] *Zhang et al.* [2011] first proposed that the east-to-west differences in TEC over the US continent at midlatitude are caused by the difference in magnetic declination, which gives rise to upward and downward ion drifts across the zero declination for a given thermospheric zonal wind direction. The upward/downward field-aligned drift moves the ions to higher/lower altitudes where their recombination rate is smaller/larger and thus increases/decreases the plasma density of the *F* region [*Rishbeth*, 1998]. Later, they analyzed the zonal wind climatology above Millstone Hill and found it to be perfectly consistent with what is expected based on the electron density difference between the east and west sides of the site [*Zhang et al.*, 2012a]. For comparison, it is valuable to examine this mechanism over the Far East region, which also has large geomagnetic declination but smaller than that of the US.

[21] Figure 10a shows that the morning vertical component of the field-aligned ion drift Vz_{zonal} (positive for upward drift) during June 2011 at midlatitude is up to –8 m/s on the east side (135°E) of the zero declination longitude and +6 m/s on the west side (60°E). According to [*Zhang et al.*, 2011,

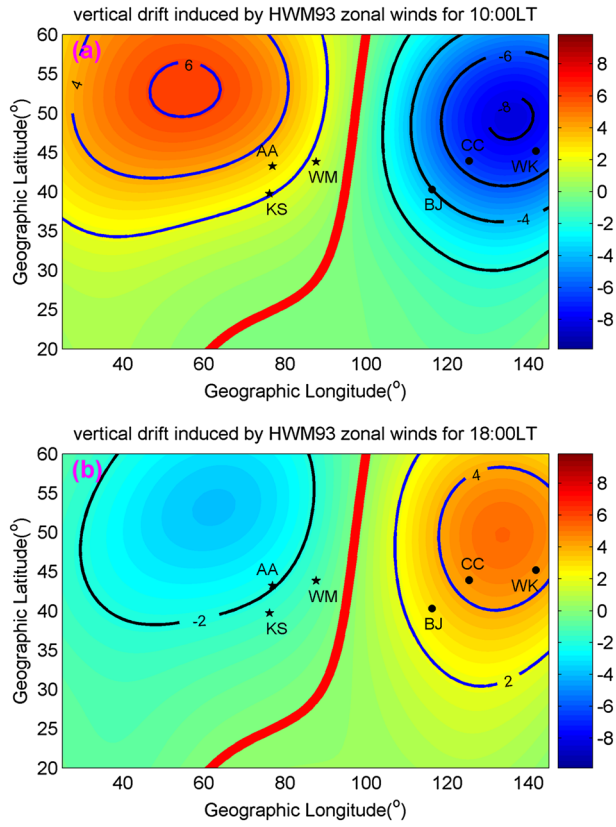

Figure 10. Vertical ion drift Vz_{zonal} derived from HWM93 zonal wind for LT = 09:00 and 18:00 under condition DOY = 152 and F10.7 = 70, superimposed with geomagnetic declination contour and the stations used in Figure 1.

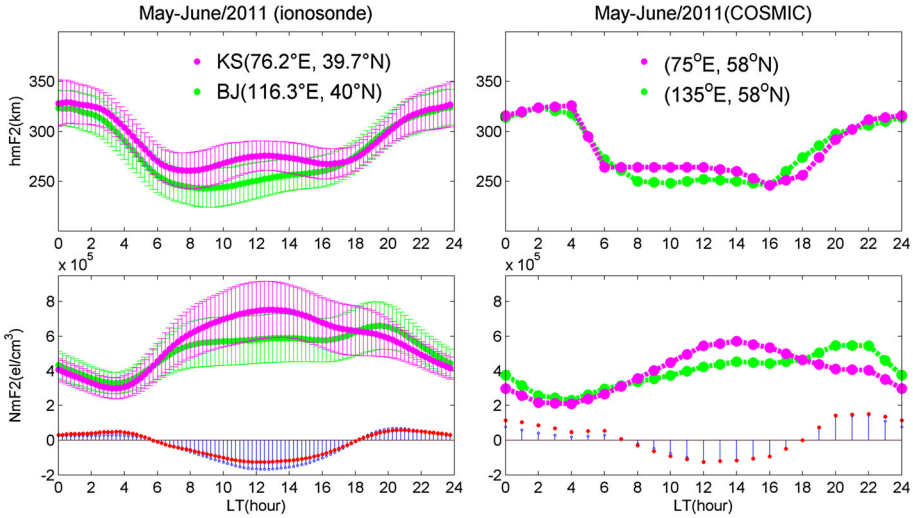

Figure 11. (left) Diurnal variations of the monthly mean hmF2 and foF2 at BJ (green) and KS (magenta) during May–June/2011. The blue empty circle denotes the ΔNmF2 ($NmF2_{BJ} - NmF2_{KS}$) while the red dot refers to the east-to-west differential index $R_{ew} \times 5 \times 10^5$. (right) Corresponding COSMIC results.

2011], Vz_{zonal} is calculated using $-Ue \sin D \cos I \sin I$, D and I are the geomagnetic declination and inclination derived from the 11th generation of International Geomagnetic Reference Field. *Ue* is the zonal winds derived from HWM93 model [*Hedin et al.*, 1996] with positive for eastward. Note that *Ue* has very small longitude variability in this region with absolute maximum east-west difference not exceeding 5 m/s, less than 5% of the mean value. Within 30 min, the 14 m/s difference in Vz_{zonal} can approximately cause 25 km differences in the height of *F* layer. Figure 11 (left) depicts the foF2 and hmF2 changes for ionosonde stations Beijing (116.3°E, 40°N) and Kashi (76.2°E, 39.7°N) during May–June 2011 while Figure 11 (right) gives the COSMIC-derived results at point (135°E, 58°N) and (75°E, 58°N). The 58°N is where the most severe positive east-west discrepancy exists as indicated in Figure 8. It is seen from the

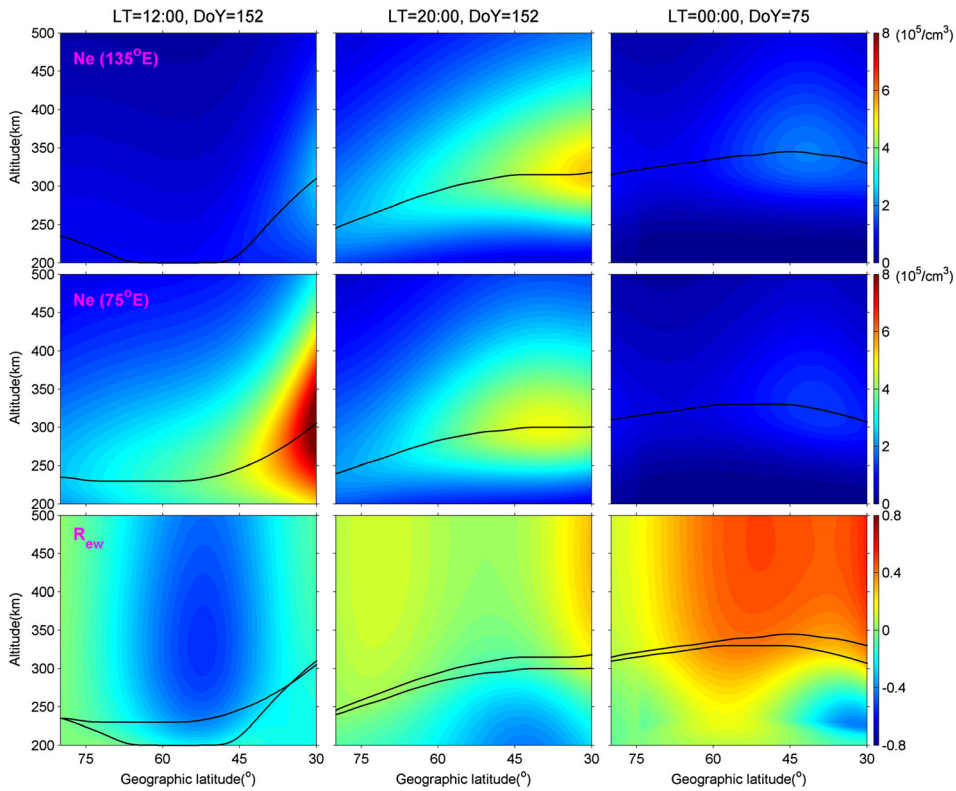

Figure 12. From top to bottom are the columns of IRI_Ne profiles at longitude 135°E, 75°E, and east-to-west differential index R_{ew} between two longitudes for LT = 10:00, 20:00 on 1 June 2011 and LT = 00:00 on 16 March, superimposed with hmF2.

figure that during 08:00–14:00 LT, the hmF2 on the west side is 25 km (ionosonde, 40°N) and 16 km (COSMIC, 58°N) higher than that of the east part, and hence results in the large negative disparity in NmF2 between east and west, which indirectly proves that the zonal neutral wind is the critical driver for the east-west difference observed in the midlatitude of the Far East region. However, zonal neutral wind seems not to possibly explain the positive correlation between the magnitude of negative R_{ew} and solar activity. The daytime westward zonal wind is shown to diminish as the solar activity increase due to the enhanced ion-drag as seen from the CHAMP measurement [*Liu et al.*, 2006]. Thus, other mechanisms, for example the longitude dependence of chemical composition, may need to be considered in the future study.

[22] At afternoon-evening hours, the direction of the zonal wind are reversed but with smaller value compared with the daytime as illustrated in Figure 10b. The Vz_{zonal} at midlatitude is up to 5 m/s on the east side (130°E) and –3 m/s on the west side (65°E), and hence produce 14 km difference in the peak height between east and west sides leading to positive R_{ew} after sunset as shown in Figure 11. The problem lies in that the positive R_{ew} during DOY 60–300 shown in Figure 3 cannot be explained alone by the thermospheric zonal wind. In comparison, nighttime R_{ew} of the US region is much larger (>0.5) and prevails over the entire winter at fixed altitude 400 km [*Zhang et al.*, 2012b]. This feature in a different way has been investigated by *Luan et al.* [2008], which revealed that the winter midnight enhancement of the Eastern American area is clearly stronger than any other longitudes. In fact, *Clilverd et al.* [1991] found corresponding longitude changes in the plasmasphere, which showed a maximum December/June ratio of N_{eq} at $L = 2.5$ with geomagnetic field line footprint located at middle to high-latitudes of ~300°E geographic longitude. The distribution has been explained by the largest offset of the geomagnetic field configuration relative to geographic coordinates as well as the largest negative declination in the eastern US sector, which result in that the conjugate area of the Southern Hemisphere ionosphere is sunlit and the ion density stays high throughout the summer providing strong downward flux for the northern winter hemisphere at midnight [*Richard et al.*, 2008]. However, the above mechanism cannot explain the observed positive R_{ew} over the Far East region because it occurs in March and June. The formation of MSNA, negative geomagnetic declination around 135°E maximizing the equatorward wind uplifting effect when sunlight still exists and in combination with downward diffusion from the plasmasphere, may explain positive R_{ew} over the summer season, while the positive R_{ew} around March needs a further study.

4.3. Features Captured by International Reference Ionosphere

[23] The International Reference Ionosphere (IRI) model describes monthly average ionospheric parameters such as electron number density, electron temperature, ion composition, ion drift, and total electron content. The main source of experimental data of IRI is based on the worldwide network of ionosondes. Because the IRI model assimilates realistic observations, it is worthwhile to see if the observed east-west difference over the Far East region is presented in or not. Although the IRI-2011 has been released (http://www.IRI.gsfc.nasa.gov), we use the version IRI-2007, of which the electron number density profile above the F2 layer maximum has already been improved [*Bilitza and Reinisch*, 2008]. Figure 12 from top to bottom shows the IRI outputs of Ne profiles along 135°E and 75°E, differential index R_{ew} during noontime 12:00 LT, evening 20:00 LT in June, and 00:00 LT in March 2006. In comparison with the COSMIC results in Figure 6 and ionosonde results in Figure 3, the latitude-altitude distribution in R_{ew} captures the summer noontime negative discrepancy and March nighttime positive difference but fails to reproduce the summer nighttime positive R_{ew} at midlatitude areas. In addition, the IRI_hmF2 is shown 20–30 km lower than that of the observation. *Hsu et al.* [2011] showed that the IRI successfully generates the MSNA at a global scale. Here for the Far East region, IRI has partly shown its ability to grasp the regional longitude difference. Thus, more data of the Far East region, especially over China, are needed to be incorporated in IRI that makes it a highly regional standard for the calculation of ionospheric parameters in research and applied problems.

5. Summary and Conclusion

[24] This study focuses on the longitudinal variations of the ionospheric electron content over the Far East areas. The feature of east-west asymmetry reported in the US region has also been revealed in the Eastern Hemisphere but with significant differences, based on the comprehensive analysis of the ground- and space-based measurements. The results show that the negative east-west difference (West side Ne > East side Ne) in the noontime is more pronounced during late spring and summer period while the evening-night positive difference (West side Ne < East side Ne) is much less significant than that of US continent. The observed diurnal variation of longitude difference can be explained roughly by the thermospheric zonal winds. Meanwhile, some new issues were raised, for example, what is the reason for the difference of solar activity and seasonal variations in the east-west asymmetry, clearly altitude-dependent, between the above two regions. The climatology changes in east-west asymmetry are obviously related to the annual and semiannual variations of the *F* region at midlatitude. The semiannual variation is pronounced in the Far East region and the annual in the US continent [e.g., *Zhao et al.*, 2007], explained by the near-pole and far-pole theory [*Rishbeth*, 1998]. Thus, a detailed comparison on the climatology features as well as mechanism between the US and the Far East region is needed.

[25] **Acknowledgments**. This research was supported by the National Natural Science Foundation of China (41174138, 41131066), the National Important Basic Research Project of China (2011CB811405), the Open Research Program of the State Key Laboratory of Space Weather. A part of this work is based on observations with the Langmuir probe, ISL, on the DEMETER satellite (CNES). The authors thank J. P. Lebreton, the PI of ISL, for the use of the data.

References

Bilitza, D., and B. W. Reinisch (2008), International Reference Ionosphere 2007: Improvements and new parameters, *Adv. Space Res.*, *42*, 599–609, doi:10.1016/j.asr.2007.07.048.

Burns, A. G., Z. Zeng, W. Wang, J. Lei, S. C. Solomon, A. D. Richmond, T. L. Killen, and Y.-H. Kuo (2008), The behavior of the F2 peak ionosphere over the South Pacific at dusk during quiet summer condition from COSMIC data, *J. Geophys. Res.*, *113*, A12305, doi:10.1029/2008JA013308.

Burns, A. G., S. C. Solomon, W. Wang, A. D. Richmond, G. Jee, C. H. Lin, C. Rocken, and Y. H. Kuo (2011), The summer evening anomaly and conjugate effects, *J. Geophys. Res.*, *116*, A01311, doi:10.1029/2010JA015648.

Chen, C. H., J. D. Huba, A. Saito, C. H. Lin, and J. Y. Liu (2011), Theoretical study of the ionospheric Weddell Sea Anomaly using SAMI2, *J. Geophys. Res.*, *116*, A04305, doi:10.1029/2010JA015573.

Chen, C. H., A. Saito, C. H. Lin, and J. Y. Liu (2012), Long-term variations of the nighttime electron density enhancement during the ionospheric midlatitude summer, *J. Geophys. Res.*, *117*, A07313, doi:10.1029/2011JA017138.

Clilverd, M. A., A. J. Smith, and N. R. Thomson (1991), The annual variation in quiet time plasmaspheric electron density determined from whistler mode group delays, *Planet. Space Sci.*, *39*, 1059–1067.

Dickinson, R. E., E. C. Ridley, and R. G. Roble (1981), A three dimensional general circulation model of the thermosphere, *J. Geophys. Res.*, *86*, 1499–1512, doi:10.1029/JA086iA03p01499.

Dudeney, J. R., and W. R. Piggott (1978), Antarctic ionospheric research, in Upper Atmosphere Research in Antarctica, Ant. Res. Ser., vol. 29, edited by L. J. Lanzerotti and C. G. Park, pp. 200–235, AGU, Washington, D. C., doi:10.1029/AR029p0200.

England, S. L. (2011), A review of the effects of non-migrating atmospheric tides on the earth's low-latitude ionosphere, *Space Sci. Rev.*, doi:10.1007/s11214-011-9842-4.

Evans, J. V. (1965), Cause of the midlatitude evening increase in foF2, *J. Geophys. Res.*, *70*, 1175–1185, doi:10.1029/JZ070i005p01175.

Hagan, M. E., A. Maute, R. G. Roble, A. D. Richmond, T. J. Immel, and S. L. England (2007), Connections between deep tropical clouds and Earth's ionosphere, *Geophys. Res. Lett.*, *34*, L20109, doi:10.1029/2007GL030142.

He, M., L. Liu, W. Wan, B. Ning, B. Zhao, J. Wen, X. Yue, and H. Le (2009), A study of the Weddell Sea Anomaly observed by FORMOSAT-3/COSMIC, *J. Geophys. Res.*, *114*, A12309, doi:10.1029/2009JA014175.

He, M., L. Liu, W. Wan, and B. Zhao (2011), A study on the nighttime midlatitude ionospheric trough, *J. Geophys. Res.*, *116*, A05315, doi:10.1029/2010JA016252.

Hedin, A. E., et al. (1996), Empirical wind model for the upper, middle and lower atmosphere, *J. Atmos. Terr. Phys.*, *58*, 1421–1447, doi:10.1016/0021-9169(95)00122-0.

Horvath, I., and E. A. Essex (2003), The Weddell Sea Anomaly observed with the TOPEX satellite data, *J. Atmos. Sol. Terr. Phys.*, *65*(6), 693–706, doi:10.1016/S1364-6826(03)00083-X.

Hsu, M. L., C. H. Lin, R. R. Hsu, J. Y. Liu, L. J. Paxton, H. T. Su, H. F. Tsai, P. K. Rajesh, and C. H. Chen (2011), The O I 135.6 nm airglow observations of the midlatitude summer nighttime anomaly by TIMED/GUVI, *J. Geophys. Res.*, *116*, A07313, doi:10.1029/2010JA016150.

Immel, T. J., E. Sagawa, S. L. England, S. B. Henderson, M. E. Hagan, S. B. Mende, H. U. Frey, C. M. Swenson, and L. J. Paxton (2006), Control of equatorial ionospheric morphology by atmospheric tides, *Geophys. Res. Lett.*, *33*, L15108, doi:10.1029/2006GL026161.

Jee, G., A. G. Burns, Y.-H. Kim, and W. Wang (2009), Seasonal and solar activity variations of the Weddell Sea Anomaly observed in the TOPEX total electron content measurements, *J. Geophys. Res.*, *114*, A04307, doi:10.1029/2008JA013801.

Karpachev, A. T., and N. A. Gasilov (2001), Zonal and meridional wind components derived from Intercosmos 19 hmF2 measurements, *Adv. Space Res.*, *27*(6-7), 1245–1252.

Karpachev, A. T., and N. A. Gasilov (2006), Causes of longitude-latitudinal variations in the ionospheric F2-layer maximum in summer nighttime conditions, *Int. J. Geomagn. Aeron.*, *6*, GI2006, doi:10.1029/2005GI000112.

Kohl, H., and J. W. King (1967), Atmospheric winds between 100 and 700 km and their effects on the ionosphere, *J. Atmos. Terr. Phys.*, *29*, 1045–1062, doi:10.1016/0021-9169(67)90139-0.

Lebreton, J. P., S. Stverak, P. Travnicek, M. Maksimovic, D. Klinge, S. Merikallio, D. Lagoutte, B. Poirier, Z. Kozacek, M. Salaquarda (2006), The ISL Langmuir Probe experiment and its data processing onboard DEMETER: scientific objectives, description and first results, *Planet. Space Sci.*, *54*, 5, doi:10.1016/j.pss.2005.10.017.

Lin, C. H., J. Y. Liu, C. Z. Cheng, C. H. Chen, C. H. Liu, W. Wang, A. G. Burns, and J. Lei (2009), Three-dimensional ionospheric electron density structure of the Weddell Sea Anomaly, *J. Geophys. Res.*, *114*, A02312, doi:10.1029/2008JA013455.

Lin, C. H., C. H. Liu, J. Y. Liu, C. H. Chen, A. G. Burns, and W. Wang (2010), Midlatitude summer nighttime anomaly of the ionospheric electron density observed by FORMOSAT-3/COSMIC, *J. Geophys. Res.*, *115*, A03308, doi:10.1029/2009JA014084.

Liu, H., S. V. Thampi, and M. Yamamoto (2010), Phase reversal of the diurnal cycle in the midlatitude ionosphere, *J. Geophys. Res.*, *115*, A01305, doi:10.1029/2009JA014689.

Liu, H., H. Lühr, S. Watanabe, W. Köhler, V. Henize, and P. Visser (2006), Zonal winds in the equatorial upper thermosphere: Decomposing the solar flux, geomagnetic activity, and seasonal dependencies, *J. Geophys. Res.*, *111*, A07307, doi:10.1029/2005JA011415.

Liu, L., B. Zhao, W. Wan, B. Ning, M.-L. Zhang, and M. He (2009), Seasonal variations of the ionospheric electron densities retrieved from Constellation Observing System for Meteorology, Ionosphere, and Climate mission radio occultation measurements, *J. Geophys. Res.*, *114*, A02302, doi:10.1029/2008JA013819.

Luan, X., and S. C. Solomon (2008), Meridional winds derived from COSMIC radio occultation measurements, *J. Geophys. Res.*, *113*, A08302, doi:10.1029/2008JA013089.

Luan, X., W. Wang, A. Burns, S. C. Solomon, and J. Lei (2008), Midlatitude nighttime enhancement in F region electron density from global COSMIC measurements under solar minimum winter condition, *J. Geophys. Res.*, *113*, A09319, doi:10.1029/2008JA013063.

Ren, Z., W. Wan, L. Liu, H. Le, and M. He (2012), Simulated midlatitude summer nighttime anomaly in realistic geomagnetic fields, *J. Geophys. Res.*, *117*, A03323, doi:10.1029/2011JA017010.

Richards, P. G., T. Chang, and R. H. Comfort (2000), On the causes of the annual variation in the plasmaspheric electron density, *J. Atmos. Sol. Terr. Phys.*, *62*, 935–946.

Rishbeth, H., and O. K. Garriott (1969), Introduction to Ionospheric Physics, Academic, San Diego, Calif.

Rishbeth, H., S. Ganguly, and J. C. G. Walker (1978), Field-aligned and field-perpendicular velocities in the ionospheric F2-layer, *J. Atmos. Terr. Phys.*, *40*, 767–784.

Rishbeth, H. (1998), How the thermospheric circulation affects the ionospheric F2-layer, *J. Atmos. Sol. Terr. Phys.*, *60*, 1385–1402.

Schreiner, W., S. Sokolovskiy, C. Rocken, and D. Hunt (1999), Analysis and validation of GPS/MET radio occultation data in the ionosphere, *Radio Sci.*, *34*, 949–966, doi:10.1029/1999RS900034.

Schreiner, W., C. Rocken, S. Sokolovskiy, S. Syndergaard, and D. Hunt (2007), Estimates of the precision of GPS radio occultations from the COSMIC/FORMOSAT-3 mission, *Geophys. Res. Lett.*, *34*, L04808, doi:10.1029/2006GL027557.

Thampi, S., C. H. Lin, H. Liu, and M. Yamamoto (2009), First tomographic observations of the midlatitudes summer night anomaly (MSNA) over Japan, *J. Geophys. Res.*, *114*, A10318, doi:10.1029/2009JA014439.

Wu, J., Z. H. Cao, and K. H. Quan (1998), Observations of the longitude effects in the mid-latitude ionospheric F region and comparisons with models, *ACTA Chinese J. Space Sci.*, *18*(2), 132–140.

Yue, X., W. S. Schreiner, Y.-C. Lin, C. Rocken, Y.-H. Kuo, and B. Zhao (2011), Data assimilation retrieval of electron density profiles from radio occultation measurements, *J. Geophys. Res.*, *116*, A03317, doi:10.1029/2010JA015980.

Zhang, S.-R., J. C. Foster, A. J. Coster, and P. J. Erickson (2011), East-West Coast differences in total electron content over the continental US, *Geophys. Res. Lett.*, *38*, L19101, doi:10.1029/2011GL049116.

Zhang, S.-R., A. J. Coster, J. M. Holt, J. C. Foster, and P. J. Erickson (2012a), Ionospheric longitudinal variations at midlatitudes: Incoherent Scatter Radar Observation at Millstone Hill, SCIENCE CHINA Technological Sciences, doi:10.1007/s11431-012-4784-y.

Zhang, S.-R., J. C. Foster, J. M. Holt, P. J. Erickson, and A. J. Coster (2012b), Magnetic declination and zonal wind effects on longitudinal differences of ionospheric electron density at midlatitudes, *J. Geophys. Res.*, *117*, A08329, doi:10.1029/2012JA017954.

Zhao, B., W. Wan, L. Liu, T. Mao, Z. Ren, M. Wang, and A. B. Christensen (2007), Features of annual and semiannual variations derived from the global ionospheric maps of total electron content, *Ann. Geophys.*, *25*, 2513–2527.

Zhao, B., W. Wan, X. Yue, L. Liu, Z. Ren, M. He, and J. Liu (2011), Global characteristics of occurrence of an additional layer in the ionosphere observed by COSMIC/FORMOSAT-3, *Geophys. Res. Lett.*, *38*, L02101, doi:10.1029/2010GL045744.